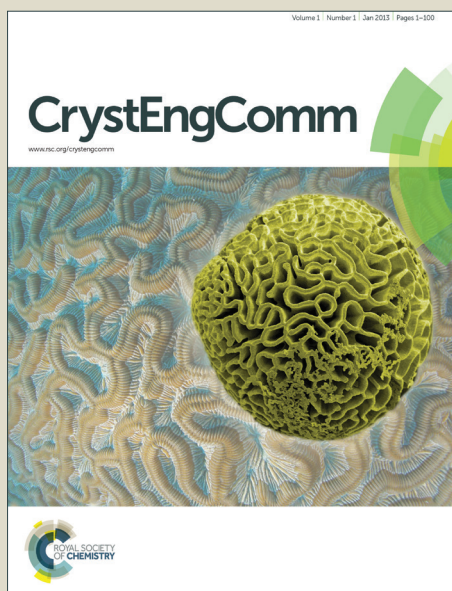


# CrystEngComm

Accepted Manuscript



This is an *Accepted Manuscript*, which has been through the Royal Society of Chemistry peer review process and has been accepted for publication.

*Accepted Manuscripts* are published online shortly after acceptance, before technical editing, formatting and proof reading. Using this free service, authors can make their results available to the community, in citable form, before we publish the edited article. We will replace this *Accepted Manuscript* with the edited and formatted *Advance Article* as soon as it is available.

You can find more information about *Accepted Manuscripts* in the [Information for Authors](#).

Please note that technical editing may introduce minor changes to the text and/or graphics, which may alter content. The journal's standard [Terms & Conditions](#) and the [Ethical guidelines](#) still apply. In no event shall the Royal Society of Chemistry be held responsible for any errors or omissions in this *Accepted Manuscript* or any consequences arising from the use of any information it contains.

Cite this: DOI: 10.1039/c0xx00000x

www.rsc.org/xxxxxx

ARTICLE TYPE

## Li<sub>2</sub>CO<sub>3</sub> thin films fabricated by sputtering techniques: the role of temperature on their properties

Lander Rojo,<sup>\* a,b</sup> Irene Castro-Hurtado,<sup>a,b</sup> María C. Morant-Miñana,<sup>b</sup> Gemma García Mandayo<sup>a,b</sup> and Enrique Castaño<sup>a,b</sup>

Received (in XXX, XXX) Xth XXXXXXXXX 20XX, Accepted Xth XXXXXXXXX 20XX  
DOI: 10.1039/b000000x

The physical and electrochemical characterization of Li<sub>2</sub>CO<sub>3</sub> thin films allows for an improved understanding of their behaviour in electrochemical devices. Firstly, the Li<sub>2</sub>CO<sub>3</sub> deposition process by RF magnetron sputtering is described. Afterwards, X-ray diffraction (XRD), atomic force microscopy (AFM) and electrochemical impedance spectroscopy (EIS) characterization techniques are employed to study the influence of temperature on the material. This way, the optimal annealing temperature as well as the optimal operating temperature of Li<sub>2</sub>CO<sub>3</sub> is determined. In light of the obtained results, it is concluded that a fabrication annealing temperature of 600 °C and an optimal operating temperature of 350 °C is set.

### Introduction

The increasingly restrictive laws regarding the emission of certain contaminant agents like CO<sub>2</sub> in various settings such as residences, the gas and automotive industries, and the natural environment makes the development of new devices that are sensitive to these agents under the conditions established today by law, indispensable. This, together with the trend of manufacturing miniaturized, low-cost and high performance devices makes thin film fabrication techniques a good choice for tackling this challenge and expanding the possible uses of different materials such as lithium carbonate (Li<sub>2</sub>CO<sub>3</sub>). Lithium carbonate is a very versatile compound due to its use in different fields such as medicine and engineering. Moreover, regarding its ionic behaviour, its properties allow it to be employed as electrode passivation film in lithium ion batteries,<sup>1</sup> as an additive to improve other electrode material behavior,<sup>2</sup> or as a key component in electrochemical devices like fuel cells or chemical sensors. In these kinds of devices, because of its ionic conductivity and high reactivity to CO<sub>2</sub>, Li<sub>2</sub>CO<sub>3</sub> can be used as solid electrolyte<sup>3,4</sup> or as sensing layer.<sup>5-7</sup> This kind of devices have been also reported with other carbonate materials such as sodium carbonate, Na<sub>2</sub>CO<sub>3</sub><sup>8-11</sup>, or binary carbonate systems.<sup>11-13</sup> The low solubility in water of Li<sub>2</sub>CO<sub>3</sub> comparing to other alkali metal carbonates makes the Li<sub>2</sub>CO<sub>3</sub> an interesting material for applications where humidity is present.<sup>14</sup> Some studies have tried to shed light on the behaviour and electrical conductivity of Li<sub>2</sub>CO<sub>3</sub>, especially in terms of observing its influence as solid electrolyte interphase (SEI) in Li ion batteries.<sup>15,16</sup> To our knowledge, few studies reported in the literature describe the characterization of Li<sub>2</sub>CO<sub>3</sub> thin films.<sup>1</sup> Thin film techniques, such as sputtering, allows fabricating miniaturized devices that have smaller size, smaller amount of material and lower power consumption comparing to other devices fabricated by bulk or

thick film techniques. In this study, little details are described about the fabrication process and characterization of the Li<sub>2</sub>CO<sub>3</sub> thin film as sensing layer. In electrochemical sensors, the sensing layer plays a key role in the operation of this kind of solid state sensor. Therefore, it is essential to select an optimal fabrication process as well as understand the temperature influence on the microstructure, surface and conduction mechanism of Li<sub>2</sub>CO<sub>3</sub>.

This work is focused on the fabrication process of Li<sub>2</sub>CO<sub>3</sub> thin films by sputtering techniques and the influence of temperature on their physical and electrochemical characterization. Parameters like surface roughness, crystallinity and temperature influence or activation energy are essential to characterize the use of Li<sub>2</sub>CO<sub>3</sub> in several approaches. Electrochemical impedance spectroscopy (EIS) is used to describe the physicochemical processes involved in the conduction through a solid state ionic conductor like Li<sub>2</sub>CO<sub>3</sub>.

### Experimental

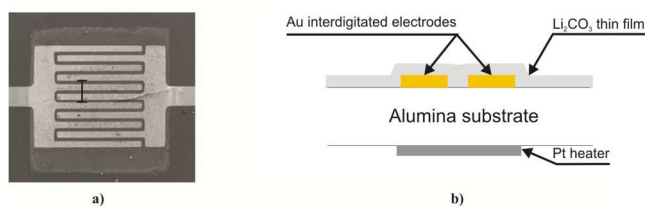
#### Li<sub>2</sub>CO<sub>3</sub> layer fabrication

Li<sub>2</sub>CO<sub>3</sub> thin film deposition were performed from a high purity Li<sub>2</sub>CO<sub>3</sub> target (99.9% Testbourne) by RF magnetron sputtering (Pfeiffer Classic 500) on a polished Al<sub>2</sub>O<sub>3</sub> substrate with a surface roughness of 5 nm and in an entire CO<sub>2</sub> atmosphere. The masks used for the photolithographic process are manufactured by Microlithography Services. The film is a polyester based 007" thick material and the black area is the photosensitive coating after it has been developed through the processing stage. The Li<sub>2</sub>CO<sub>3</sub> layer was patterned as a square of 1.5 mm x 1.5 mm with an average thickness of 200 nm measured with a KLA Tencor profilometer. The reason for using this atmosphere was to prevent the co-deposition of Li<sub>2</sub>O that is produced by the decomposition of Li<sub>2</sub>CO<sub>3</sub> in Li<sub>2</sub>O and CO<sub>2</sub> (Li<sub>2</sub>CO<sub>3</sub> ⇌ Li<sub>2</sub>O + CO<sub>2</sub>),<sup>1</sup> and in this way shift this reaction to the left. A water-free lift-off process

was required for the  $\text{Li}_2\text{CO}_3$  patterning procedure. High purity DMSO (Dimethyl sulfoxide,  $\text{C}_2\text{H}_6\text{OS}$ , Sharlau) was used as solvent in the lift-off process. Its higher boiling point compared to other commonly used solvents prevents the condensation of water during the lift off process by avoiding the dissolution of  $\text{Li}_2\text{CO}_3$  in the residual water. Due to the high ionic conduction temperature of  $\text{Li}_2\text{CO}_3$ , a thermal treatment was necessary to stabilize the microstructure of  $\text{Li}_2\text{CO}_3$  film and avoid any possible phase transition during high temperature operation. To set the optimal thermal treatment temperature, the layers were heated at several temperatures, 200 °C, 400 °C and 600 °C, in a  $\text{CO}_2$  atmosphere for 2 hours (ATV PEO 601 furnace) and then cooled to room temperature to study the influence of the annealing temperature on the material.

### 15 Electrochemical cell fabrication

With regard to EIS measurements, electrical connections and a heater had to be included to the  $\text{Li}_2\text{CO}_3$  thin film to let an integrated electrochemical cell be formed by Au electrodes and a Pt heater. A 200 nm-thick Pt heater was deposited by DC magnetron sputtering (Edwards coating system E306A) on the bottom part of the  $\text{Al}_2\text{O}_3$  substrate. The heater provides the different temperatures to the  $\text{Li}_2\text{CO}_3$  in this EIS study. Following this step, 200 nm-thick Au interdigitated electrodes with a finger width of 50  $\mu\text{m}$  were deposited by RF magnetron sputtering (Edwards coating system E306A) on the top part of the  $\text{Al}_2\text{O}_3$  substrate. Au electrodes were selected instead of Pt electrodes due to the high reactivity of Pt with  $\text{Li}_2\text{CO}_3$ .<sup>6</sup> Then, an annealing treatment of 500 °C was applied for 2 hours to stabilize both metallic layers. Finally, in order to get the electrochemical cell, the  $\text{Li}_2\text{CO}_3$  thin film is deposited using the fabrication process described above. Figure 1 shows the top view (a) and cross section (b) of the  $\text{Li}_2\text{CO}_3$  electrochemical cell.



35 **Fig. 1** Image of the sputtered electrochemical cell. a) Top view of  $\text{Li}_2\text{CO}_3$  thin film over Au interdigitated electrodes and b) cross section of the  $\text{Li}_2\text{CO}_3$  cell used for the electrochemical characterization of the lithium carbonate.

### 40 Characterization methods

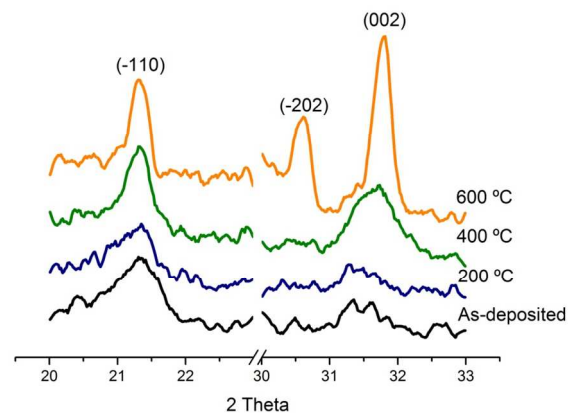
The crystallographic structure of the  $\text{Li}_2\text{CO}_3$  films before and after their thermal treatment was analyzed by X-ray diffraction (XRD) by means of a Philips XPERT MRD diffractometer in a glancing angle configuration ( $\text{Cu K}\alpha_1$   $\lambda = 1.54059$  Å). The obtained patterns have been slightly smoothed with the Savitzky-Golay algorithm with 5 points of window. A JPK NanoWizard atomic force microscope in the intermittent contact mode using a Silicon tip ( $r < 10$  nm; Aspect ratio  $< 6:1$ ) with a force constant of 40  $\text{Nm}^{-1}$  and a resonant frequency of approximately 300 kHz was

50 employed to study the topography of the material under test. The EIS analysis was performed with a Solartron 1260 frequency response analyzer in the frequency range of 0.1 Hz -1 MHz and an applied amplitude of 200 mV. The data was obtained and processed with Zview and Zplot tools. Afterwards, the obtained 55 impedance patterns were fitted with an equivalent circuit in order to quantitatively analyze the obtained results.

## Results and discussion

It is well known that amorphous ceramic films are less stable than the crystalline ones. For this reason, the influence of the 65 annealing temperature on the crystallization process was investigated using XRD and AFM. In this section, the results concerning the XRD diffraction are described. Figure 2 shows a detail of the evolution of the XRD patterns of as-deposited and annealed  $\text{Li}_2\text{CO}_3$  thin films at three different annealing temperatures. The complete XRD pattern is presented in the SI. It is important to note that the intensity of the peaks (-110), (-202) and (002) directions are growing as a function of the annealing temperature. The obtained Bragg peaks are characteristic of a monoclinic structure with a (002) preferred orientation (checked 70 against ICDD: 00-022-1141) in accordance with other studies reported in the literature.<sup>17</sup> The data processing has served to obtain the following lattice parameters:  $a = 8.377$  Å,  $b = 4.974$  Å,  $c = 6.194$  Å and  $\beta = 114.72^\circ$ .

The comparison of the diffraction patterns shows that a 75 nanocrystalline structure is obtained with a crystallite size increasing with the thermal treatment. From the Scherrer formula a value of 17 nm and 27 nm average crystallite size has been calculated for the samples treated at 400 °C and 600 °C, respectively. The as-deposited samples and the samples annealed 80 at 200 °C do not show sufficiently defined peaks to estimate the average crystallite size. The (-202) peak remains unaltered except for the samples treated at 600 °C, where a considerable texturization process takes place. The intensity of the peak (002) increases dramatically at this temperature, as Figure 2 illustrates. 85 However, the temperature influence on the (-110) Bragg peaks is much lower.



90 **Fig. 2**  $\text{Li}_2\text{CO}_3$  diffraction pattern of peaks (-110), (-202) and (002) for the annealing temperatures of 200 °C, 400 °C, 600 °C and as-deposited samples. Only the spectra where the peaks of  $\text{Li}_2\text{CO}_3$  are present is represented.

A suitable role of the fabricated  $\text{Li}_2\text{CO}_3$  thin films might be to

work as a sensitive layer, an electrolyte or a SEI in different kind of thin film electrochemical devices. Taking into account the surface reactions that takes place in this kind of materials, it is evident that the particle size, shape and roughness of the material are critical factors in the behaviour of  $\text{Li}_2\text{CO}_3$ . Figure 3 a-b reflects a great difference between the topography of the as-deposited samples and the samples treated at 600 °C. The difference in the morphology and topography of  $\text{Li}_2\text{CO}_3$  is related to the influence of the annealing temperature. The absence of holes in the as-deposited films is evidenced in Figure 3a (see cross section in SI). Moreover, the as-deposited samples and the samples treated at 200 °C and 400 °C, to a lesser extent, present some protuberances that disappear completely at 600 °C. This phenomenon could be related to mechanical stresses that arise during the deposition process.

Figures 3 c-f reveal the evolution of the surface of  $\text{Li}_2\text{CO}_3$  with the annealing temperature. The increase in particle size as a function of the temperature can be observed in the images. The roughness calculated from scans over several micrometers is an important parameter<sup>18,19</sup> because this factor can affect the behaviour under  $\text{CO}_2$  due to the increase of the exposed area when it is employed as sensing layer or its behaviour as SEI layer in batteries. In general, the roughness presents increasing values with the annealing temperature, when is calculated in small areas (2  $\mu\text{m} \times 2 \mu\text{m}$ ). In contrast, a different behaviour is observed

when larger areas are analyzed. The as-deposited samples show a surface with a RMS roughness of 415.9 Å. This relative large roughness of the film is attributed to the previously mentioned protuberances. The samples treated at 200 °C and 400 °C present an RMS roughness of 205.3 Å and 142.9 Å, respectively. Finally, the samples annealed at 600 °C exhibit a value of 425.3 Å RMS roughness. The evolution of the RMS roughness with annealing temperature is represented in the supporting information. It is important to note that this annealing temperature produces protuberance-free films with a large roughness value can be explained by the film being crystalline.<sup>20</sup>

The new arrangement of the particles may be described by an Ostwald ripening process that produces an increment in the observed particles size.<sup>21-23</sup> An average particle size of 54.4 nm  $\pm$  7.7 nm, 108.2 nm  $\pm$  19.5 nm, 156.7 nm  $\pm$  22.8 and 381.9 nm  $\pm$  74.26 nm has been obtained for the as deposited samples and the samples treated at 200 °C, 400 °C and 600 °C. Therefore, the 600 °C thermal treatment is suitable when a more uniform surface and more reproducible films are needed due to the absence of the protuberances. Moreover, this high annealing temperature assures microstructure stabilization up to 600 °C which gives a wide operating temperature range to  $\text{Li}_2\text{CO}_3$  which cannot be obtained with a lower annealing temperature.

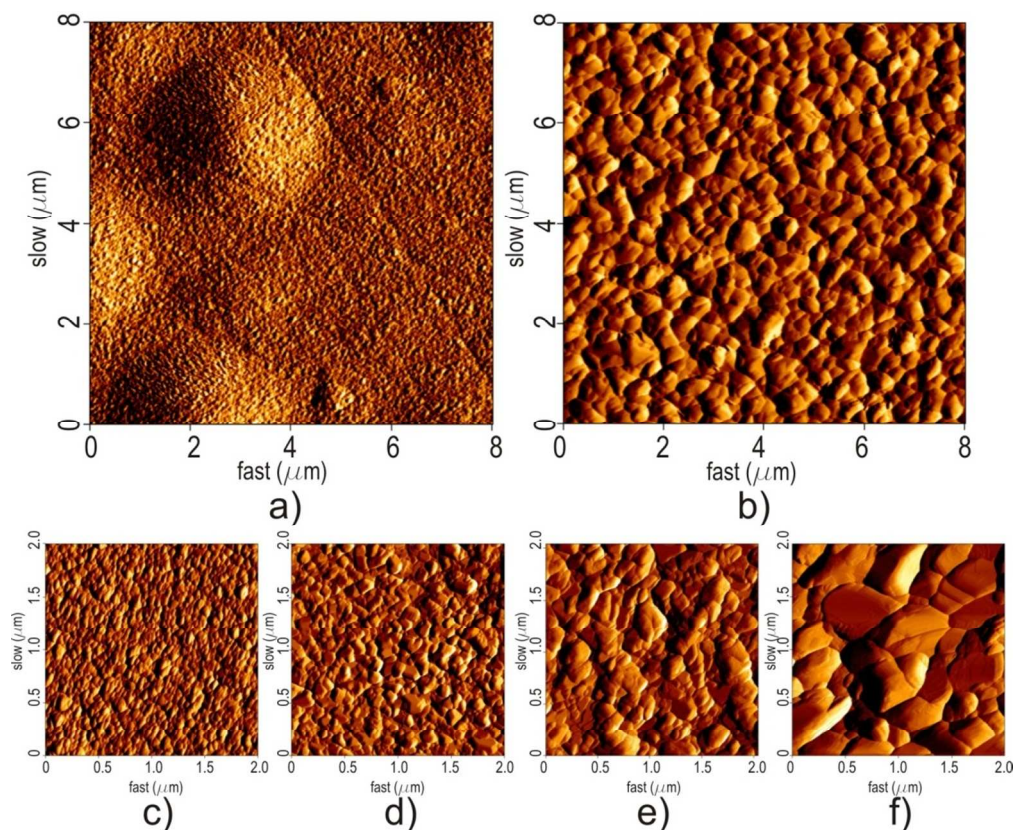


**Fig. 3** AFM lock in amplitude pictures of a) as deposited sample and b) sample treated at 600 °C. AFM lock in amplitude pictures of c) as deposited samples treated at d) 200 °C, e) 400 °C and f) 600 °C.

The EIS technique is used to study the performance of ionic conductors such as  $\text{Li}_2\text{CO}_3$  and observe the influence of different factors, like temperature, on their conduction mechanisms. This

analysis was carried out on the samples annealed at 600 °C and in a  $\text{CO}_2$  atmosphere, to study the behaviour of  $\text{Li}_2\text{CO}_3$  and draw some conclusions regarding its optimal operating temperature.

The impedance spectra obtained between 200 °C and 425 °C are plotted in Figure 5.  $\text{Li}_2\text{CO}_3$  impedance spectra do not present any change on their shape influenced by temperature. Only the high frequency arc is shown due to the irrelevance of the low frequency arc, corresponding to the electrodes, for the  $\text{Li}_2\text{CO}_3$  characterization purpose. The impedance spectra presented in Figure 4 only display the high frequency part of the low temperature arcs due to their high impedance value. Complete spectra are added in the supporting information. The arcs present a slight depression (in other words, their centers are under the X axis) which means a distribution in the relaxation frequency, mainly produced by surface roughness, thickness inhomogeneities or composition, and non-uniform current distribution.

In order to quantitatively analyze the results presented by the impedance spectra, an equivalent circuit (EC) must fit the experimental spectra. The selected EC is represented in the inset of Figure 4 and it is composed of an  $\text{Rp}||\text{C}$  parallel circuit in series with an  $\text{Rs}$ .  $\text{Rs}$  represents the resistance of the connections. The parallel an  $\text{Rp}||\text{C}$  circuit represents the conduction mechanism involved in the conduction through the  $\text{Li}_2\text{CO}_3$  layer. A constant phase element, CPE, is extensively used in EC for experimental data fitting instead of a capacitor owing the frequency dispersion revealed by the latter.<sup>24</sup> However, first tests with a CPE element showed a CPE exponent near 1. This confirms the fully capacitive behaviour of the cell and therefore, the possibility for using a capacitor in the EC. Moreover, the results show depression angles below 8°, which confirms this procedure.

The values obtained from the fitting of Figure 4 spectra using the EC model are listed in Table 1. The impedance decreases until the temperature reaches 350 °C where the impedance starts increasing again. This phenomenon might be explained by the disruption of  $\text{Li}_2\text{CO}_3$  films due to temperature process. The  $\text{Rp}$  decreases near to four orders of magnitude from the point of maximum impedance (200 °C) to the point of minimum impedance (350 °C). This value describes the conductivity maximum of  $\text{Li}_2\text{CO}_3$  thin film, which serves to select the optimum operating temperature of  $\text{Li}_2\text{CO}_3$  thin films for future applications. Interestingly, the C values have a similar evolution as  $\text{Rp}$  but in a lesser extent.

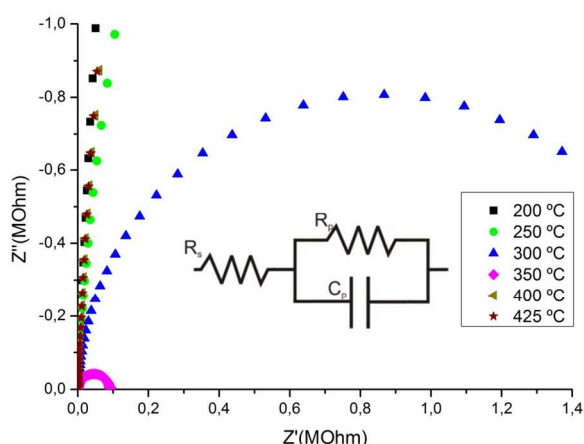


**Fig. 4**  $\text{Li}_2\text{CO}_3$  impedance spectra in the temperature range of 200 °C- 425 °C. Only high frequency arcs, with respect to  $\text{Li}_2\text{CO}_3$ , are plotted in the spectra. Simplified electrical equivalent circuit used for the impedance spectra fitting. The  $\text{Rs}$  represents the resistance presented by the connections and the  $\text{Rp}||\text{C}$  circuit describes the conduction across  $\text{Li}_2\text{CO}_3$ .

**Table 1** Values from the EC circuit of the  $\text{Li}_2\text{CO}_3$  samples at different test temperature.

Test temperature (°C)	$\text{Rp}$ (MOhm)	C (F)
200	348.35	3.5236 E-11
250	17.63	3.1458 E-11
300	1.70	2.8825 E-11
350	0.090	2.8075 E-11
400	28.611	2.8869 E-11
425	38.758	2.9185 E-11

The dependency of the resistance on temperature is represented in the Arrhenius graph in Figure 5. This kind of graphs normally consist of a line with two slopes which describes two different behaviors: the intrinsic region and the extrinsic region. The high temperature region, or intrinsic region, describes the contribution of the migration of the charge carrier and the thermal formation of new defects. In this region the activation energy is given by Equation 1.<sup>25</sup>

$$E_a = W + \frac{1}{2} W_f \quad (1)$$

where  $E_a$  is the activation energy,  $W$  is the migration energy and  $W_f$  is the formation energy. The low temperature region, or extrinsic region, depends on the impurity concentration and represents the conduction that is dominated by the mobility of extrinsic defects. In this region, the  $W_f$  has no influence; therefore the activation energy is due only to the migration energy ( $E_a = W$ ). Regarding  $\text{Li}_2\text{CO}_3$  conduction, it is known that the Li ion migration in monoclinic  $\text{Li}_2\text{CO}_3$  is given by the diffusion of the Li ion through interstitial positions (Frenkel defects<sup>4,16,26</sup>). The reported migration energies of Li ion are between 0.34 and 0.6 eV depending on the diffusion path of the charge carrier.<sup>15</sup> Regarding the formation energy ( $W_f$ ), a 1.12 eV and 1.7 eV has been reported by different authors.<sup>15,27</sup> Thus, taking into account the low melting temperature of bulk  $\text{Li}_2\text{CO}_3$  (720 °C) and the test temperature range (200 °C – 450 °C), we assume that the graph represented in Figure 5 corresponds to the intrinsic region of the conduction of  $\text{Li}_2\text{CO}_3$ . Taking the highest and lowest values of  $W$  and  $W_f$  reported in the literature and following Equation 1, an  $E_a$  range between 0.9 eV and 1.45 eV is expected. A 1.50 eV  $\pm$  0.06 eV average activation energy was obtained from the slope of the fitting represented by the continuous line of the low temperature region. The agreement between the activation energies expected and the obtained experimental values confirms the utility of the sputtered  $\text{Li}_2\text{CO}_3$  thin films.

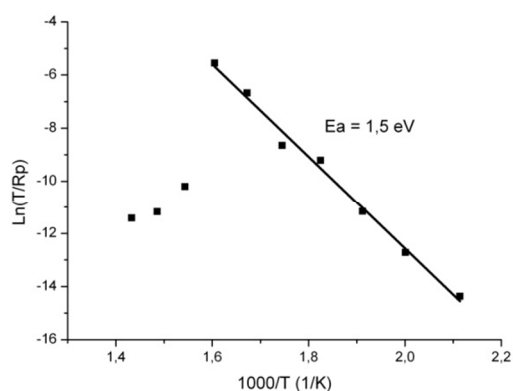
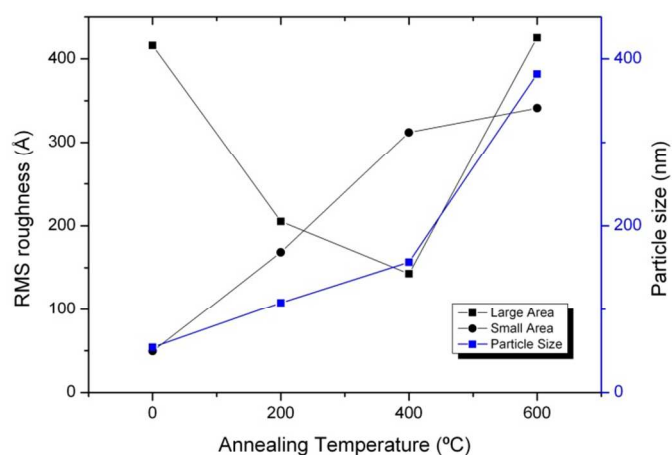


Fig. 5 Arrhenius plot of  $\text{Li}_2\text{CO}_3$  samples. The continuous line represents the linear fitting performed to obtain the slope.



Supporting 1. Evolution of the RMS roughness and particle size of  $\text{Li}_2\text{CO}_3$  thin films with annealing temperature. The included lines in the graph try to show more clearly the evolution of the roughness and particle size with the annealing temperature.

## Conclusions

The fabrication process of  $\text{Li}_2\text{CO}_3$  thin film by RF magnetron sputtering has been described. The strategy involved in the fabrication process is the deposition of  $\text{Li}_2\text{CO}_3$  in an entire  $\text{CO}_2$  atmosphere and the patterning process of the  $\text{Li}_2\text{CO}_3$  thin films in a complete absence of water. A thermal treatment temperature of 600 °C is the optimal one because more crystalline, uniform and reproducible surfaces are obtained. Moreover, this high temperature (600 °C) provides a wide operating temperature range to  $\text{Li}_2\text{CO}_3$  for EIS analysis.

The EIS analysis has revealed the evolution of the impedance of  $\text{Li}_2\text{CO}_3$  thin films with temperature presenting an impedance minimum around 350 °C. This value discloses the conductivity maximum of the sputtered  $\text{Li}_2\text{CO}_3$  thin films.

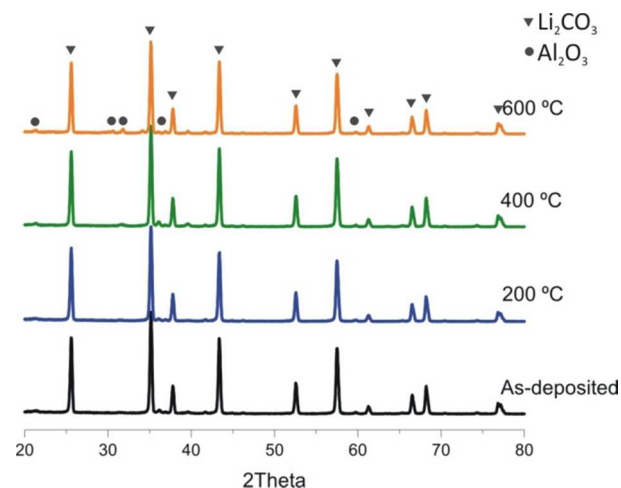
This work supposes the first steps of thin film solid state electrochemical devices development based on  $\text{Li}_2\text{CO}_3$ . One of the applications of these sensors is to provide inexpensive devices with a wider  $\text{CO}_2$  detection range than other systems in addition to setting up an alternative to more expensive techniques such as gas chromatography or optical detection in the  $\text{CO}_2$  sensing field. Moreover, owing the low melting temperature of this material, the application field will be found in low and mid operating temperature devices.

## Notes and references

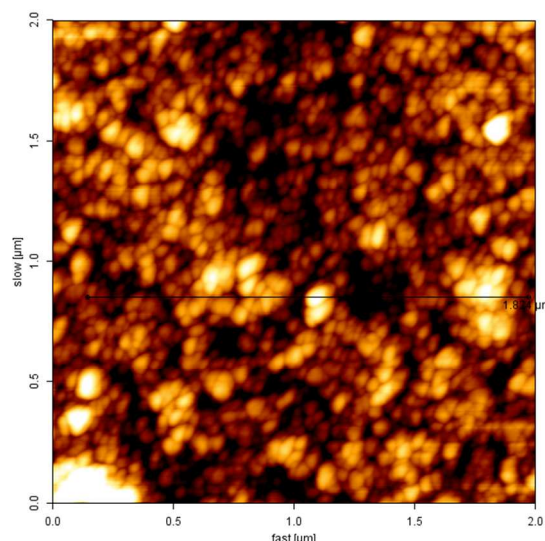
- <sup>a</sup> CEIT, Paseo Manuel de Lardizabal 15, 20018 Donostia-San Sebastián, Spain, lrojo@ceit.es  
<sup>b</sup> CIC microGUNE, Goiru Kalea 9 Polo Innovación Garaia, 20500 Arrasate-Mondragón, Spain

† Electronic Supplementary Information (ESI) available:

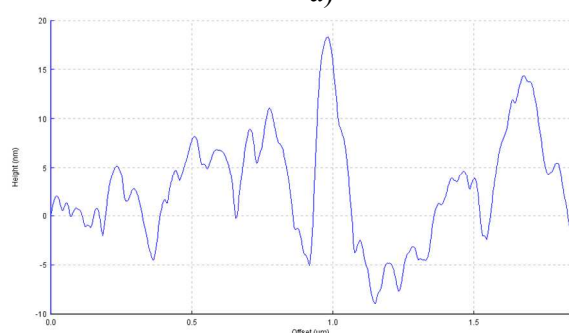
35



Supporting 2 Complete diffraction pattern of  $\text{Li}_2\text{CO}_3$ .

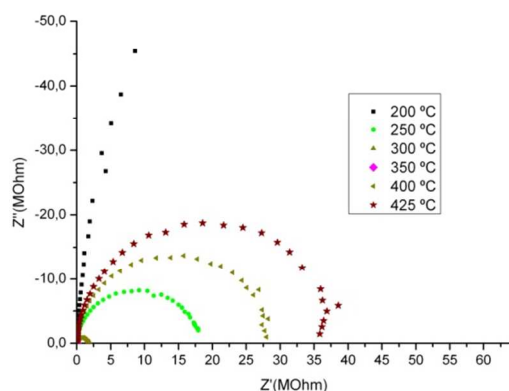


a)



b)

5 **Supporting 3.** AFM height image and its cross section of an as deposited sample



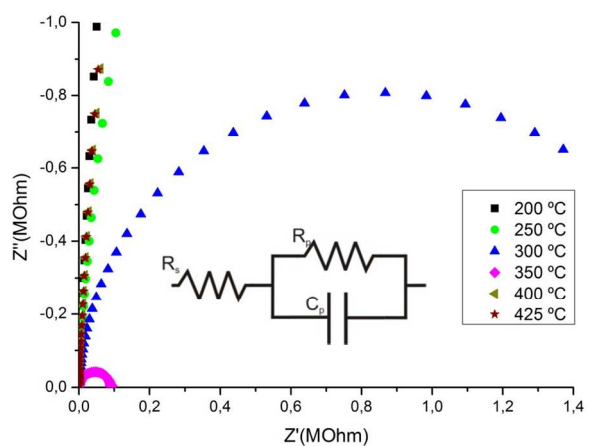
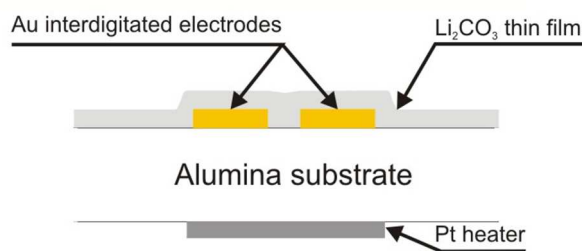
10 **Supporting 4**  $\text{Li}_2\text{CO}_3$  impedance spectra in the temperature range of 200 °C–425 °C.

‡Funding for this work was provided by the Ministry of Science and Education of Spain within the framework of the NAMIRIS project no. TEC2010-21375-C05-01 “Modular system based on advanced micro and  
15 nanotechnologies for safety and air-quality applications”.

1. W. C. West, J. Whitacre, B. V. Ratnakumar, E. Brandon, J. O. Bloisi, and S. Surampudi, 1997, vol. 791, pp. 1997–1997.
2. J. Shin, C. Han, U. Jung, S. Lee, H. Kim, and K. Kim, *J. Power Sources*, 2002, **109**, 47–52.
- 20 3. Y. can Zhang, H. Tagawa, S. Asakura, J. Mizusaki, and H. Narita, *Solid State Ionics*, 1997, **100**, 275–281.
4. J. Mizusaki, H. Tagawa, K. Saito, K. Uchida, and M. Tezuka, *Solid State Ionics*, 1992, **56**, 791–797.
- 25 5. Y. Shimamoto, T. Okamoto, Y. Itagaki, H. Aono, and Y. Sadaoka, *Sensors Actuators B Chem.*, 2004, **99**, 113–117.
6. M. Wierzbicka, P. Pasierb, and M. Rekas, *Phys. B Condens. Matter*, 2007, **387**, 302–312.
7. Y. Zhu, W. Chu, and W. Weppner, *Chinese Sci. Bull.*, 2009, **54**, 1334–1339.
- 30 8. H. Näfe, *Sensors Actuators B Chem.*, 2000, **69**, 46–50.
9. J. W. Fergus, *Sensors Actuators B Chem.*, 2008, **134**, 1034–1041.
10. J. Lee, *J. Eur. Ceram. Soc.*, 2004, **24**, 1431–1434.
- 35 11. J. Lee, *Sensors Actuators B Chem.*, 2003, **96**, 663–668.
12. N. Miura, S. Yao, Y. Shimizu, and N. Yamazoe, *Measurement*, 1992, **9**, 165–170.
13. H. S. Hong, J. W. Kim, S. J. Jung, and C. O. Park, *Sensors Actuators B Chem.*, 2006, **113**, 71–79.
- 40 14. T. Kida, K. Shimanoe, N. Miura, and N. Yamazoe, *Sensors Actuators B Chem.*, 2001, **75**, 179–187.
15. H. Iddir and L. A. Curtiss, *J. Phys. Chem*, 2010, 20903–20906.
16. M. Park, X. Zhang, M. Chung, G. B. Less, and A. M. Sastry, *J. Power Sources*, 2010, **195**, 7904–7929.
- 45 17. P. Pasierb, R. Gajerski, M. Rokita, and M. Rekas, *Phys. B Condens. Matter*, 2001, **304**, 463–476.
18. F. Ruffino, M. Grimaldi, F. Giannazzo, F. Roccaforte, and V. Raineri, *Nanoscale Res. Lett.*, 2009, **4**, 262–8.
19. A.-L. Barabási and H. E. Stanley, *Fractal Concepts in Surface Growth*, 1995.
- 50 20. M. Putkonen, T. Aaltonen, M. Alnes, T. Sajavaara, O. Nilsen, and H. Fjellvåg, *J. Mater. Chem.*, 2009, **19**, 8767.
21. D. L. Beke, Yu.S., and Kaganovskii, *Mater. Sci. Eng.*, 1995, **32**, 185–199.
- 55 22. I. Beszeda, E. G. Gontier-Moya, and Á. W. Imre, *Appl. Phys. A*, 2005, **81**, 673–677.

- 
23. F. Ruffino, A. Canino, M. G. Grimaldi, F. Giannazzo, F. Roccaforte, and V. Raineri, *J. Appl. Phys.*, 2008, **104**, 024310.
24. J. Jorcin, M. Orazem, N. Pebere, and B. Tribollet, *Electrochim. Acta*, 2006, **51**, 1473–1479.
- 5 25. J. M. Albella Martin and J. M. Martinez Duart, *Física de dieléctricos*, Marcombo, Barcelona, 1984.
26. S. Zhuiykov, *Sensors (Peterborough, NH)*.
27. S. Shi, Y. Qi, H. Li, and L. G. Hector, *J. Phys. Chem.*, 2013, **117**, 8579–8593.

10



This work supposes the first step for the use of sputtered  $\text{Li}_2\text{CO}_3$  thin films for their use in electrochemical devices.